Material Selection for Accident Tolerant Fuel Cladding

B.A. PINT, K.A. TERRANI, Y. YAMAMOTO, and L.L. SNEAD

Alternative cladding materials to Zr-based alloys are being investigated for accident tolerance, which can be defined as >100X improvement (compared to Zr-based alloys) in oxidation resistance to steam or steam-H_2 environments at ≥1473 K (1200 °C) for short times. After reviewing a wide range of candidates, current steam oxidation testing is being conducted on Mo, MAX phases, and FeCrAl alloys. Recently reported low-mass losses for Mo in steam at 1073 K (800 °C) could not be reproduced. Both FeCrAl and MAX phase Ti_2AlC form a protective alumina scale in steam. However, commercial Ti_2AlC that was not single phase, formed a much thicker oxide at 1473 K (1200 °C) in steam and significant TiO_2, and therefore, Ti_2AlC may be challenging to form as a cladding or a coating. Alloy development for FeCrAl is seeking to maintain its steam oxidation resistance to 1748 K (1475 °C), while reducing its Cr content to minimize susceptibility to irradiation-assisted α' formation. The composition effects and critical limits to retaining protective scale formation at >1673 K (1400 °C) are still being evaluated.

© ASM International (ASM) and The Minerals, Metals & Materials Society (TMS) 2015

I. INTRODUCTION

SINCE the nuclear accident in Japan in 2011,[1,2] considerable research has been devoted to identify light water reactor (LWR) fuel systems that tolerate severe accident scenarios (*i.e.*, beyond design basis accidents).[3–9] The objective is to provide larger safety margins, *i.e.*, delay the onset of severe LWR core degradation by reducing the rate of H_2 and heat generated by the rapid oxidation of Zr-base alloy cladding and increase the coping time after an accident.[7–9] Thus, one of the key criteria for new fuel cladding is to identify materials with oxidation rates ≥100X slower than Zr-base alloys.[7]

Various Fe-Cr, Fe-Cr-Ni, and Fe-Cr-Al alloys have been evaluated for this application as well as SiC and Mo. Recently, the latter was reported to have better steam oxidation resistance than previously reported.[10] Alumina-forming materials represent an attractive option, including FeCrAl-type alloys and MAX phase compositions, such as Ti_2AlC.[11,12] This study reports the ranking of the reaction kinetics of the various classes of alloys and the current status of steam oxidation behavior of Mo, Ti_3SiC_2, Ti_2AlC, and FeCrAl alloys, the latter being a promising candidate where the focus is on alloy development to improve its tensile properties while retaining steam oxidation resistance to 1748 K (1475 °C). Previously, the effect of steam pressure (up to 20.7 bar) and H_2 additions was investigated and found to have limited effect on the oxidation behavior of the most oxidation-resistant alloys.[3,4] Therefore, the steam oxidation results reported in this study were conducted at 1 bar.

B.A. PINT, Group Leader and Distinguished Research and Development Staff, and Y. YAMAMOTO, Research and Development Staff, are with the Materials Science and Technology Division, Oak Ridge National Laboratory, Oak Ridge TN 37831-6156. Contact e-mail: pintba@ornl.gov K.A. TERRANI, Research and Development Staff and ORNL FCRD Program Manager, is with the Fusion & Materials for Nuclear Systems Division, Oak Ridge National Laboratory. L.L. SNEAD, formerly a Corporate Fellow and FCRD Program Manager, is with the Materials Science and Technology Division, Oak Ridge National Laboratory.

II. EXPERIMENTAL PROCEDURE

Specimens evaluated in this study were coupons typically ~1.5-mm thick and 4 to 5 cm^2 in surface area with compositions given in Table I in mass pct. Unfortunately there was not sufficient MAX phase material to obtain chemical compositions of those specimens by the same inductively coupled plasma & combustion analytical techniques. Commercial alloys evaluated included La_2O_3-dispersed Mo (Rhenium Alloys Moly LX) and three MAX phases: commercial Ti_3SiC_2 and Ti_2AlC and high-purity laboratory-produced Ti_2AlC. The model FeCrAl alloys were typically cast at ORNL followed by hot rolling and annealing at 973 K (700 °C). The Fe13Cr5AlY alloy was extruded at 1323 K (1050 °C) followed by a 1 hour annealing at 973 K (700 °C). The 2nd generation FeCrAl alloys were hot-rolled (C135) or

hot-extruded (C135Nb) at 1073 K (800 °C) followed by annealing at 1073 K (800 °C) for 1 hour. Oxidation experiments were conducted in three different systems: (1) thermal gravimetric analysis (TGA) in 1 bar of Ar-50 pct H_2O or dry air at 1473 K (1200 °C), using a Cahn model 1000 microbalance with a quartz tube, (2) magnetic suspension TGA using a Rubotherm DynTHERM LP-HT-II instrument where the alumina test chamber was fully isolated with dry air or 100 pct steam at 1073 K to 1773 K (800 °C to 1500 °C), and (3) a high-temperature [maximum 1973 K (1700 °C)] test rig consisting of a vertical alumina tube with two resistively heated furnaces where steam or air entered the bottom of the tube and was preheated to 1273 K to 1573 K (1000 °C to 1300 °C) by the first furnace and the specimen was held in the second furnace in an alumina holder attached to the top tube using an alumina pin.[13] For the TGA experiments, the specimen was suspended with a Pt-Rh wire, which experienced little evaporation in steam or Ar-50 pct H_2O. The deionized water used to generate steam was not Ar-bubbled or filtered as is typically done for ~873 K (600 °C) steam testing, thus the O_2 content was ~10 ppm. At 1473 K (1200 °C), the equilibrium O_2 partial pressure in 1 bar steam was calculated as ~125 ppm O_2. However, at 1073 K (800 °C), the equilibrium O_2 level is <1 ppm. The gas velocity in the TGA experiments was typically 1 to 2 cm/s while the steam velocity was 5 to 60 cm/s in the high-temperature furnace. The mass change of all specimens was measured using a Mettler Toledo model XP205 balance with ±0.04 mg or ±0.01 mg/cm^2 accuracy. After exposure, specimens were metallographically sectioned and examined by light microscopy. More extensive characterization of the reaction products has

been provided elsewhere[4,14] or will be provided in future publications. Tensile properties were measured at 573 K (300 °C) in laboratory air using SS-3 sub-sized sheet specimens (25-mm long, gage of 0.8×5 mm) with a strain rate of 10^{-3}/s.

III. RESULTS AND DISCUSSION

Figure 1 provides an overview of the steam oxidation kinetic data of the various fuel cladding candidates.[4,13,15–17] The data were fitted to an Arrhenius relationship

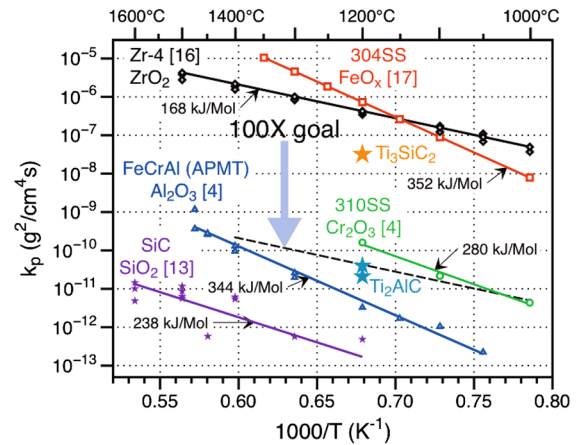Fig. 1—Arrhenius plot of the steam oxidation rate constants for various candidate materials[4,13,15–17] with the resulting oxidation activation energies noted. Current results for MAX phase materials are also shown.

Table I. Alloy Compositions (Mass Pct and ppmw) Determined by Inductively Coupled Plasma & Combustion Techniques

Alloy	Fe	Zr	Ni	Cr	Al	Mo	Mn	Si	C	O	S	Other
Zircaloy-2	0.1	98.1	0.1	0.1				0.01	0.019	0.115	<	1.4Sn
Zircaloy-4	0.22	98.2	—	0.11	—	—	—	0.01	0.016	0.118	<	1.27Sn
304L			70.3	—	8.27	18.8	0.01	0.27	0.73	0.42	0.028	0.006	<
310SS	51.9	<	19.5	25.4		0.13	1.89	0.70	0.044	0.006	10	0.15Co,0.1Cu
E-Brite	72.6	0.1	25.8			1.0	<	0.2	0.003	0.003	100	0.1 V,0.1Nb
Fe15Cr5AlY	79.9	<	<	15.0	5.0	<	<	0.01	0.004	0.001	12	0.033Y
Fe13Cr5AlY	82.1	<	<	12.9	4.9	<	<	0.01	0.004	0.002	13	0.031Y
Fe13Cr5AlY-2	82.3	<	<	13.2	4.4	<	<	0.01	0.002	0.001	3	0.12Y
C135	80.9	<	<	12.7	4.2	1.9	<	0.20	0.003	0.002	7	0.031Y,0.04 W
C135C	81.0	<	<	12.5	4.2	1.9	<	0.21	0.09	0.002	5	0.026Y
C135Nb	78.2			13.3	5.2	2.1		0.22	<0.01	<50		1Nb,0.03Y
PM2000	74.6	—	0.1	18.9	5.1	0.01	0.11	0.04	0.01	0.25	8	0.37Y,0.45Ti
APMT	69.8	0.11	0.18	21.2	4.8	2.8	0.10	0.47	0.036	0.053	<3	0.21Y,0.17Hf,0.02Ti
MA956	74.2	<	0.08	20.0	4.5	<	0.08	0.07	0.015	0.199	25	0.40Y,0.37Ti
APM	73.3	0.10	—	20.4	5.5	—	0.08	0.23	0.030	0.053	10	0.03Ti, < 0.01Y
SUH21	78.6	<	0.11	17.7	3.0	0.01	0.12	0.29	0.008	0.003	<3	0.11Ti, < 3ppmY
Alkrothal 720	81.4	0.06	0.12	13.0	4.2	<	0.44	0.30	0.034	15	0.002	0.44Ti, < 3ppmY
Alkrothal 14	80.3	0.12	0.11	14.7	4.2	<	0.20	0.17	0.029	<	14	0.01Ti, < 3ppmY
Alkrothal 3	82.7	0.09	<	13.4	3.3	<	0.20	0.22	0.027	<	12	0.02Ti, < 3ppmY
Ohmaloy30	82.8	<	0.58	12.6	2.6	0.05	0.41	0.26	0.017	<	<3	0.34Ti,0.1 V
Ohmaloy40	81.7	<	0.53	12.7	3.6	0.10	0.37	0.22	0.021	<	<3	0.34Ti,0.13 V
Mo LX	0.02	<	<	0.01	<	99.3	<	0.01	0.001	0.098	<3	0.56La
CVD-SiC	—	—	0.01	—	—	—	—	69.8	30.2	0.003	<	—

< denotes below the detectable limit of 0.01 or 0.001 pct for interstitials.

$$k_p = k_o \exp(-E_a/RT), \qquad [1]$$

where k_p is the thermogravimetric parabolic rate constant (with units of g^2/cm^4 s), k_o is a constant, E_a is the activation energy, R is the gas constant, and T is temperature in Kelvin. The values fitted from the referenced data sets are shown in Table II. From Figure 1 it is clear that the reaction rates for Zr-based cladding and conventional 18Cr-8Ni stainless steel, such as type 304L, are similar because the stainless steel cannot form a protective scale in steam at these temperatures and instead rapidly oxidizes to form FeO_x. Thus, these 18Cr-8Ni austenitic steels (e.g., types 304, 321, and 347) that were previously used as LWR cladding[18] do not meet the accident tolerance criteria as they rapidly form FeO_x at <1473 K (1200 °C) in steam.[3,4]

In order to achieve a 100X improvement in oxidation resistance for Zr-based alloys, i.e., 1 μm of oxide formed rather than 100 μm, the parabolic rate constant, k_p, would need to decrease by a factor of 10^4, as shown by the dashed line in Figure 1. Higher alloyed (Ni and/or Cr) stainless steels, such as type 310 (310SS) shown in Figure 1, provide close to the desired 100X reduction due to the formation of a protective Cr_2O_3 scale in steam.[4] However, these compositions are not desirable for this application because of the high neutronic penalty of Ni.[7] The steam oxidation resistance of ferritic (12 to 25 pct Cr, <1 pct Ni) steels also was investigated but ≥22 pct Cr was required even with Mn, Si, and Y additions.[15] This level of Cr is a concern due to the potential embrittlement from α' formation during

irradiation.[7,19,20] Thus, Cr_2O_3-forming alloys have been evaluated and are potential secondary candidates for this application.

From Figure 1 it is clear that both alumina and silica scales have lower reaction rates and can remain protective to much higher temperatures. The silica scale formed on SiC has excellent steam oxidation resistance up to at least 1973 K (1700 °C)[13] but many other aspects of its utilization as nuclear fuel cladding, including thermo-mechanical reliability[21] and hydrothermal corrosion resistance, have not yet been proven sufficient.[22]

Figure 2 illustrates the rates shown in Figure 1 at 1373 K and 1473 K (1100 °C and 1200 °C) in 1 bar steam. After only 1 h at 1373 K (1100 °C), the ZrO_2 scale was >100 μm, Figure 2(a). At a higher magnification, Figure 2(b) shows the chromia scale formed on a commercial Fe-26Cr-1Mo alloy (E-Brite) after 4 hours at 1473 K (1200 °C). This alloy is shown instead of 310SS, because the chromia scale spalled from 310SS on cooling due to its higher thermal expansion mismatch between the alloy and the chromia scale.[23] Figure 2(c) shows the slower growing α-Al_2O_3 scale formed on APMT (Fe-22Cr-5Al-3Mo) after a similar 4 hours exposure at 1473 K (1200 °C).

Based on the limitations of chromia-forming steels and silica-forming ceramics, alumina-forming claddings appear to be an attractive solution for further focus. Yet recently it was suggested that the steam oxidation rate of Mo was much lower than in air and this material should be further considered.[10] These results were quite surprising and appeared to contradict decades old understanding of Mo oxidation.[24–26] In order to

Table II.   Steam Oxidation Rate Data for Materials Representing Various Classes of Candidates

| Material	Temp. Range [K (°C)]	k_o (g/cm^2 s$^{1/2}$)	E_a (kJ/mol)	Scale	References
Zirc-4	1273 to 1773 (1000 to 1500)	3.64×10^{-1}	168	ZrO_2 (tetragonal)	[16]
304SS	1273 to 1623 (1000 to 1350)	2.40×10^{6}	352	FeO_x	[17]
310SS	1273 to 1473 (1000 to 1200)	1.17	280	Cr_2O_3	[4]
APMT	1323 to 1748 (1050 to 1475)	7.84	344	Al_2O_3 (corundum)	[4,15]
SiC	1473 to 1873 (1200 to 1600)	3.81×10^{-5}	238	SiO_2 (cristobalite)*	[13]

*In H_2O environments, SiO_2 forms $Si(OH)_4$.
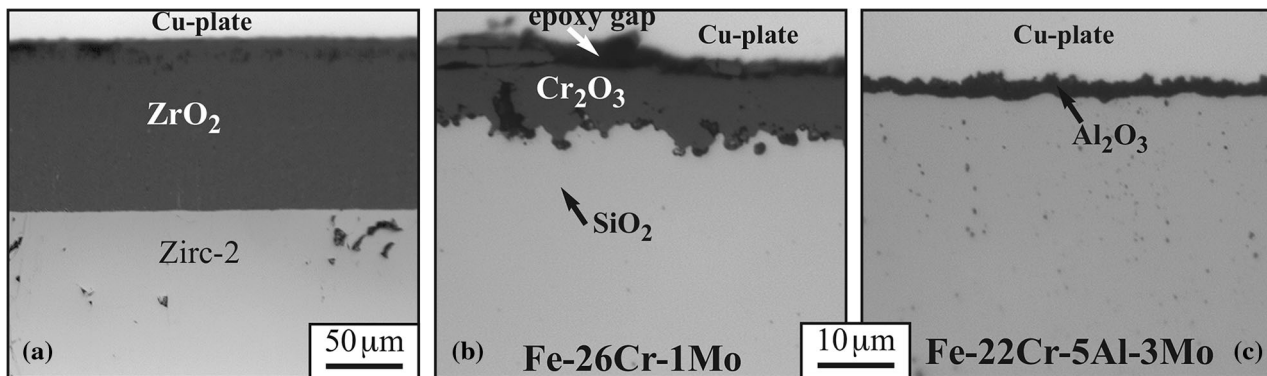
Fig. 2—Light microscopy of polished cross sections of specimens exposed to 1 bar steam (a) Zircaloy-2 tube after 1 h at 1373 K (1100 °C), (b) Fe-26Cr-1Mo coupon after 4 h at 1473 K (1200 °C), and (c) FeCrAlMo coupon after 4 h at 1473 K (1200 °C).

confirm these newer results, La_2O_3-doped Mo specimens were oxidized in steam and in air at 1073 K (800 °C) for 4 hours in the high-temperature test module. (This rig could be more easily cleaned after testing than the TGA rigs by replacing the alumina reaction tube, which became contaminated with MoO_3.) Thus, only final mass change was generated, rather than continuous mass gain curves reported in the prior study.[10] Figure 3(a) compares the results from this study after 4 hours at 1073 K (800 °C) in dry air and steam and values extrapolated to 4 h from Reference 10 at 1073 K (800 °C). In both environments, the present results showed higher mass gains than the prior study. Both studies agreed that the mass loss was reduced in steam compared to dry air. However, the present results are <3X reduction in steam compared to a >100X reduction measured previously. There are a number of differences between the two studies including the La_2O_3-doped Mo used in this study, the lower O_2 content in the steam in the prior study, and the difference in gas flow rates. Further work will be needed to study these issues and resolve the differences between the two data sets. As an example of the complexity encountered, the current results had a 5.8 cm/s gas flow rate in both environments, while the prior results had a flow rate of ~9 cm/s. Initial ORNL experiments to determine the effect of flow rate found an unusual result. Increasing the flow rate in steam to 12 cm/s resulted in a reduced mass loss (173 mg/cm²) compared to 229 mg/cm² at 5.8 cm/s at 1073 K (800 °C). Nominally it would be expected that increasing the flow rate would increase the evaporation of a volatile reaction product. However, the appearance of the former specimen suggests that the greater surface oxide retained on the surface may have inhibited mass loss, Figure 3(b). The competition between volatilization and oxide formation was noted earlier for this temperature range.[24] The effect of velocity on steam oxidation requires further study.

MAX phase ceramics are another class of potential candidates with hundreds of potential compositions.[27,28] The recent focus has been on Ti_2AlC, as an alumina-forming material that could be used as a bulk material or a coating.[11,12,29] In order to compare MAX phase performance to alumina-forming FeCrAl alloys, two commercial MAX phase materials were obtained, Ti_3SiC_2 and Ti_2AlC. Figure 4(a) shows the TGA results for these materials in steam at 1473 K (1200 °C). The Ti_3SiC_2 specimen formed a thick TiO_2-rich scale that was identified by x-ray diffraction (XRD), rather than SiO_2. In Figure 4(b), the thick oxide appears to have two layers but has not been further characterized because the high oxidation rate (3×10^{-8} g² cm⁴/s) does not meet the criteria for this application, Figure 1. This reaction product appears very similar to the previous studies in air at 1473 K (1200 °C) where the outer layer was TiO_2 and the inner layer a mixed TiO_2-SiO_2.[30]

The commercial Ti_2AlC specimen exhibited a much lower mass gain but the steady state rate constant was 4×10^{-11} g² cm⁴/s, about 10X higher than expected for an alumina-forming alloy at this temperature, Figure 1. After exposure, the Ti_3SiC_2 specimen was gold, while the Ti_2AlC specimen had some fraction of gold in the gray scale. Characterization of the scale and substrate by XRD determined that the scale was 16 vol pct TiO_2 and the substrate was 3.5 pct TiC. In cross section, the scale was not uniformly thin, Figure 4(c), further suggesting that this commercial grade material could not form a uniform alumina scale under these conditions. A high-purity Ti_2AlC (0 pct TiC detected by XRD) specimen was exposed under the same conditions and showed a much lower mass gain, Figure 4(a). The cross section shown in Figure 4(d) is much more uniform but still 5 pct TiO_2 was detected in the scale and the rate constant was 2×10^{-11} g² cm⁴/s, which is higher than the rate observed for FeCrAl, Figure 1. The presence of TiO_2 in the scale formed in air on Ti_2AlC has been previously reported.[29] Thus, even with the best processing, Ti_2AlC is difficult to fabricate commercially with the precise composition necessary to form alumina in steam at 1473 K (1200 °C), and likely will be difficult to fabricate as a thin oxidation-resistant coating on a Zr-based cladding.[31] Additional characterization and steam oxidation testing of these specimens at higher
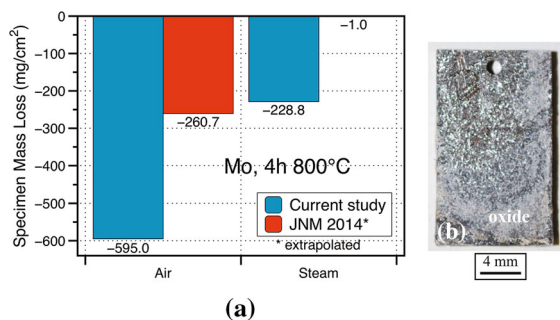

(a)

Fig. 3—(a) Comparison between the mass gain measured in this study with a 5.8 cm/s gas flow rate and La_2O_3-doped Mo specimens exposed and extrapolated values from Ref. [10] in steam and dry air for 4 h at 1073 K (800 °C), (b) image of a La_2O_3-doped Mo specimen exposed in steam for 4 h at 1073 K (800 °C) at 12 cm/s flow rate where the mass loss was only 173 mg/cm².
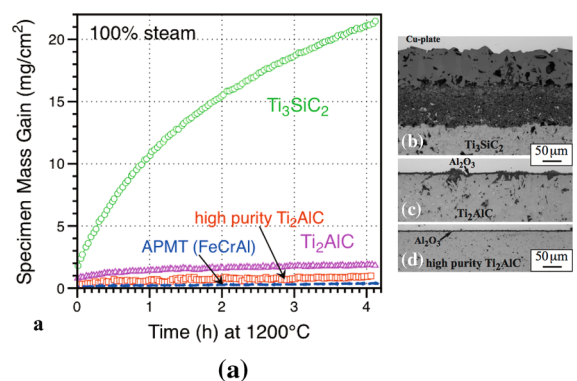

(a)

Fig. 4—(a) Mass gain as a function of exposure time to 1473 K (1200 °C) steam for three different MAX phase specimens compared to APMT (FeCrAl) and light microscopy of polished cross sections of these specimens (b) Ti_3SiC_2, (c) commercial Ti_2AlC, and (d) high-purity Ti_2AlC.

temperatures is in progress and will be reported in more detail elsewhere.

The majority of the recent work has focused on optimizing FeCrAl, which appears to have many of the features desirable for an accident tolerant fuel cladding. Most of the initial testing[3,4,14,15] was performed on conventional Fe-20Cr-5Al alloys such as APMT and PM2000, an oxide dispersion strengthened (ODS) FeCrAl that is no longer commercially available. Figure 5 shows that APMT can form a protective alumina scale even at 1748 K (1475 °C) for 4 hours exposure in steam and also in dry air. However, 4 hours at 1773 K (1500 °C) (close to the solidus temperature) in steam fully consumed the APMT specimen. The mass gain results for APMT in steam were similar in both the Rubotherm TGA and the high-temperature test module, Figure 5.

For the fuel cladding application, recent neutron irradiation results at the High Flux Isotope Reactor at ORNL of model Fe-(10 to 18 pct)Cr-Al alloys have confirmed the concern that high >14 pct Cr will result in a large number density of α' precipitates leading to potential embrittlement problems.[32] Thus, an alloy development effort has focused on identifying lower Cr FeCrAl compositions. Figure 6 is an evolving study of the effect of Cr and Al content on protective scale behavior at 1473 K (1200 °C) on both commercial and model FeCrAl alloys. Initially, evaluations were done in the Cahn TGA in Ar-50 pct H_2O[15] but more recent results were obtained in the Rubotherm TGA using 100 pct H_2O that shifted some of the results.[14] The open symbols in Figure 6 were protective, meaning they formed a slow-growing alumina scale for 4 hours in steam, while the shaded symbols formed Fe-rich oxide nodules in Ar-50 pct H_2O or 100 pct H_2O and were not considered protective, as they behaved more like the 304SS in Figure 1. The model alloys suggest that ~17.5 pct Cr is needed with 3 to 4 pct Al contents to form a protective alumina scale at 1473 K (1200 °C) in

steam. However, at lower Cr contents that are less likely to form α' during irradiation, it is clear that the Al content needs to be ≥5 pct.

Returning to Figure 5, a surprising aspect of the alloy development was that these leaner compositions were not able to form alumina at 1748 K (1475 °C) or even 1723 K (1450 °C), like APMT. Figure 5 shows that a Fe-13Cr-5Al + Y alloy was limited to 1673 K (1400 °C) [i.e., not protective at 1698 K (1425 °C)] but a Fe-15Cr-5Al + Y alloy could not form alumina at 1673 K (1400 °C) but did form a protective alumina scale at 1623 K (1350 °C). Nominally the capability should increase with increasing Cr content to the ~21 pct Cr level found in APMT. The beneficial effect of Cr on alumina scale formation is traditionally referred to as the "third" element effect but the Cr effect on the maximum use temperature has not previously been considered.[33] The issue of maximum temperature capability is still being studied through a combination of isothermal steam exposures and "ramp" testing where the specimen is exposed in the Rubotherm TGA with the temperature increasing 5 degrees/min and steam introduced at 873 K (600 °C).[14] When the specimen can no longer form a protective alumina scale, the large mass increase is detected by the TGA and the heating stopped.

Figure 7 shows an example of the current alloy development efforts to increase the 573 K (300 °C) tensile properties of a 13Cr-5Al alloy with the compositions shown in Table I. Note that a different Fe-13Cr-5Al + Y alloy was used for the oxidation testing shown in Figure 5. A larger heat with a slightly different composition was melted in order to measure the tensile properties and conduct initial tube fabrication trials. Additions of Mo and Si and variations with C and Nb, among other elements have been investigated and processed by different methods, as noted in the previous section. These
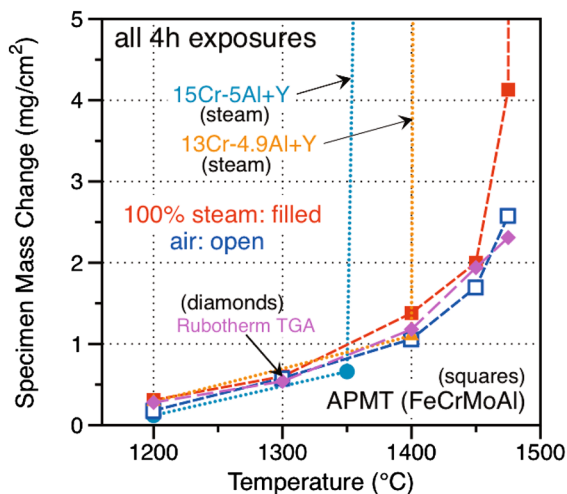

Fig. 5—Specimen mass change in 4 h exposures at each temperature in either 1 bar steam or flowing air (APMT only) for several FeCrAl alloys. Exposures were conducted in the high-temperature furnace except for the APMT data in steam from the Rubotherm TGA (diamonds) which indicated similar performance in the two systems.
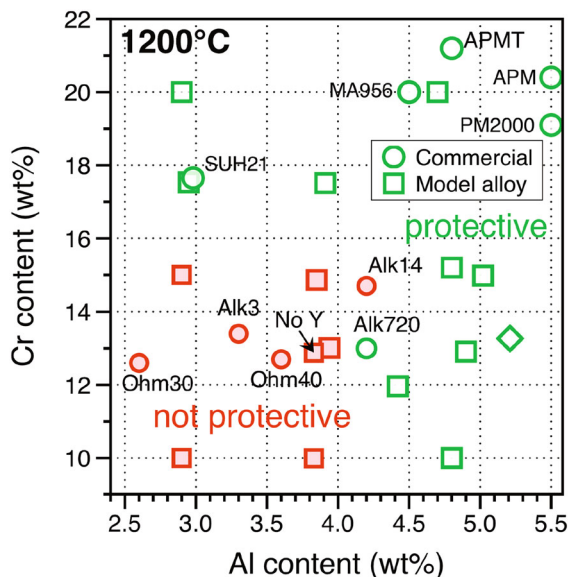

Fig. 6—Effect of Cr and Al alloy content on steam oxidation resistance at 1473 K (1200 °C) in commercial (circles) and model (squares) FeCrAl alloys, showing compositions which form a thin, protective alumina scale with open symbols and those that cannot form alumina in steam with shaded symbols.
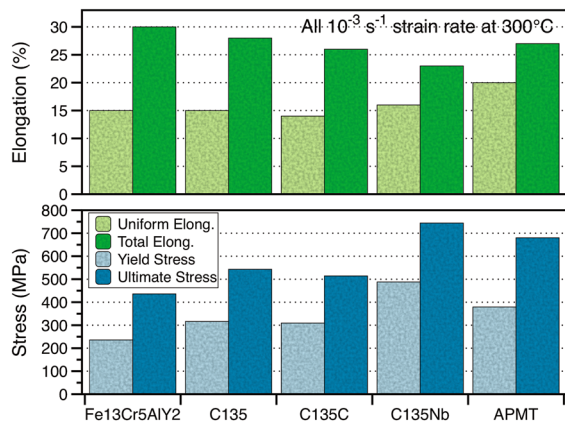
Fig. 7—Tensile properties at 573 K (300 °C) for several FeCrAl alloys with a 10^{-3}/s strain rate.
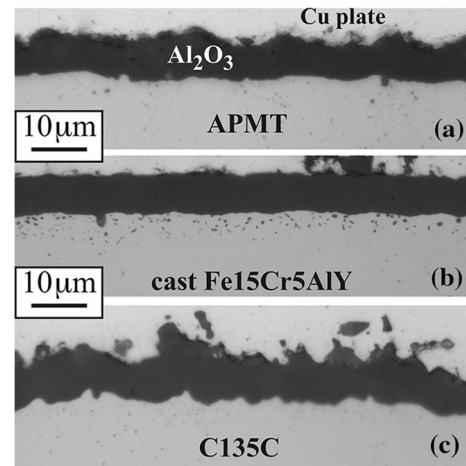

Fig. 8—Light microscopy of polished cross sections of specimens exposed to 1 bar steam at 1673 K (1400 °C) (a) APMT, (b) 1st generation Fe15Cr5AlY, and (c) 2nd generation C135C.

composition and thermal mechanical strategies to obtain improved microstructures and secondary phases that pin grain boundaries (*e.g.,* Laves phase with Nb in C135Nb[34]) have successfully increased the yield strength by 30 to 100 pct compared to the initial Fe-13Cr-5Al composition, while maintaining ductility similar to the commercial APMT alloy, Figure 7. A higher strength alloy allows for a thinner cladding wall, which minimizes the neutronics penalty for FeCrAl compared to Zr-based cladding.[7] An alternative strategy being pursued is to develop a low-Cr ODS FeCrAl alloy for this application.[35,36] In that case, the tensile properties are much higher but there is increased concern about the maximum operating temperature and the ability to fabricate thin tubing from an ODS alloy.

Maintaining the maximum temperature capability in these modified alloys remains a concern. One strategy has been to increase the Al content above 5 pct (*e.g.,* alloy C135Nb) compared to only 4.2 pct in some of the initial modified heats, Table I. Steam oxidation testing of the new alloys is still in progress but Figure 8(c) shows a protective scale formed on one of the new higher strength alloys (C135C), with a scale similar in thickness to that formed on APMT (Figure 8(a)) and a cast version of Fe-15Cr-5Al-Y (Figure 8(b)). This cast alloy, nearly identical in composition to the alloy shown in Figure 5, did form a protective scale at 1673 K (1400 °C). However, the fine oxide precipitates observed in the alloy adjacent to the scale are unusual and may suggest the onset of non-protective behavior. While FeCrAl alloys are 50+ years old,[37,38] few prior studies examined their high-temperature performance in steam or for such short time periods. Thus, these high-temperature steam oxidation conditions are unexplored until now. Previous experimental work were for applications such as heating elements or fossil-fuel power generation heat exchangers where multi-year lifetimes were desired at ~1373 K (1100 °C).[39] The ramp testing of model alloys suggests that Cr, Al, and Y are all beneficial to maximum operating temperature.[14] However, some anomalies, like that shown in Figure 5 remain, and further study is in progress. Typically, the diffusion rate of Al is considered rapid and microstructure is not an important factor, but

those assumptions may need to be revisited based on different behaviors of cast and wrought Fe-15Cr-5Al + Y, Figures 5 and 8(b).

Finally, while these results for low-Cr FeCrAl alloys are positive, a substantial amount of work remains to fabricate high-quality thin-walled tubing and demonstrate its operational performance in ~593 K (320 °C) water, *e.g.,* long-term corrosion rates, irradiation resistance, and any synergism between oxidation behavior and radiation (both at high and low temperature).

IV. SUMMARY

The high-temperature steam oxidation resistance of several alternative cladding materials was investigated for improved accident tolerance. The mass loss of La_2O_3-dispersed Mo in steam at 1073 K (800 °C) was less than in dry air, but sill very rapid. At 1473 K (1200 °C), Ti_3SiC_2 did not form a protective scale and results for Ti_2AlC suggested that single-phase laboratory material formed a slower growing alumina scale compared to commercial Ti_2AlC. Fabricating Ti_2AlC coatings will likely be a challenge for fuel cladding applications. For FeCrAl, alloy development is in progress for a Fe-13Cr-5Al base composition with improved tensile properties due to optimized composition and heat treatment. For steam oxidation resistance, one key area remaining for FeCrAl alloy development is to retain the highest temperature capability, similar to the 1748 K (1475 °C) temperature limit for the commercial FeCrAl alloy APMT.

REFERENCES

1. R. Gauntt, et al.: *Fukushima Daiichi Accident Study (Status as of April 2012)*, Sandia National Laboratory Report, SAND2012-6173, Albuquerque, NM, 2012.
2. K.R. Robb, M.W. Francis, and L.J. Ott: *Nucl. Technol.*, 2014, vol. 186, pp. 145–60.
3. T. Cheng, J.R. Keiser, M.P. Brady, K.A. Terrani, and B.A. Pint: *J. Nucl. Mater.*, 2012, vol. 427, pp. 396–400.
4. B.A. Pint, K.A. Terrani, M.P. Brady, T. Cheng, and J.R. Keiser: *J. Nucl. Mater.*, 2013, vol. 440, pp. 420–27.
5. K.A. Terrani, C.M. Parish, D. Shin, and B.A. Pint: *J. Nucl. Mater.*, 2013, vol. 438, pp. 64–71.
6. Y. Yan, J.R. Keiser, K.A. Terrani, G.L. Bell, and L.L. Snead: *J. Nucl. Mater.*, 2014, vol. 448, pp. 436–40.
7. K.A. Terrani, S.J. Zinkle, and L.L. Snead: *J. Nucl. Mater.*, 2014, vol. 448, pp. 420–35.
8. S.J. Zinkle, K.A. Terrani, J.C. Gehin, L.J. Ott, and L.L. Snead: *J. Nucl. Mater.*, 2014, vol. 2014 (448), pp. 374–79.
9. M.T. Farmer, L. Leibowitz, K.A. Terrani, and K.R. Robb: *J. Nucl. Mater.*, 2014, vol. 448, pp. 534–40.
10. A.T. Nelson, E.S. Sooby, Y.-J. Kim, B. Cheng, and S.A. Maloy: *J. Nucl. Mater.*, 2014, vol. 448, pp. 441–47.
11. J.W. Byeon, J. Liu, M. Hopkins, W. Fischer, N. Garimella, K.B. Park, M.P. Brady, M. Radovic, T. El-Raghy, and Y.H. Sohn: *Oxid. Met.*, 2007, vol. 68, pp. 97–111.
12. S. Basu, N. Obando, A. Gowdy, I. Karaman, and M. Radovic: *J. Electrochem. Soc.*, 2012, vol. 159 (2), pp. C90–96.
13. K.A. Terrani, B.A. Pint, C.M. Parish, C.M. Silva, L.L. Snead, and Y. Katoh: *J. Am. Ceram. Soc.*, 2014, vol. 97, pp. 2331–52.
14. B.A. Pint, K.A. Unocic, and K.A. Terrani: *Mater. High Temp.*, 2015, vol. 32, pp. 28–35.
15. B.A. Pint, K.A. Terrani, J.R. Keiser, M.P. Brady, Y.Yamamoto, and L.L. Snead: NACE Paper ED2013-3083, Houston, TX, Presented at the 16th Environmental Degradation conference, Asheville, NC, 2013.
16. J.V. Cathcart, R.E. Pawel, R.A. McKee, R.E. Druschel, G.J. Yurek, and J.J. Campbell et al.: Zirconium metal–water oxidation kinetics, IV: reaction rate studies, ORNL/NUREG-17, Oak Ridge National Laboratory, 1977.
17. H.C. Brassfield, J.F. White, L. Sjodahl, and J.T. Bittel: Recommended Property and Reaction Kinetics Data for Use in Evaluating a Light-Water-Cooled Reactor Loss of Coolant Incident Involving Zircaloy-4 or 304SS Clad UO_2, GEMP-482, General Electric Co., 1968.
18. A. Strasser, J. Santucci, K. Lindquist, W. Yario, G. Stern, L. Goldstein, and L. Joseph: *An Evaluation of Stainless Steel Cladding for Use in Current Design LWRs, Report NP-2642*, Electric Power Research Institute, Palo Alto, CA, 1982.
19. M.H. Mathon, Y. de Carlan, G. Geoffroy, X. Averty, A. Alamo, and C.H. de Novion: *J. Nucl. Mater.*, 2003, vol. 312, pp. 236–48.
20. G. Bonny, D. Terentyev, and L. Malerba: *Scripta Mater.*, 2008, vol. 59, pp. 1193–96.
21. M. Ben-Belgacem, V. Richet, K.A. Terrani, Y. Katoh, and L.L. Snead: *J. Nucl. Mater.*, 2014, vol. 447, pp. 125–42.
22. Y. Katoh, K.A. Terrani, and L.L. Snead: Systematic Technology Evaluation Program for SiC/SiC Composite-based Accident-Tolerant LWR Fuel Cladding and Core Structures, ORNL/TM-2014/210, Oak Ridge, TN, 2014.
23. I.G. Wright and R.B. Dooley: *Mater. High Temp.*, 2011, vol. 28, pp. 40–57.
24. E.A. Gulbransen, K.F. Andrew, and F.A. Brassart: *J. Electrochem. Soc.*, 1963, vol. 110, pp. 952–59.
25. M. Kilpatrick and S.K. Lott: *J. Phys. Chem.*, 1965, vol. 69, pp. 1638–40.
26. G.R. Belton and A.S. Jordan: *J. Phys. Chem.*, 1965, vol. 69, pp. 2065–71.
27. M.W. Barsoum: *Prog. Solid State Chem.*, 2000, vol. 28, pp. 201–81.
28. P. Eklund, M. Beckers, U. Jansson, H. Högberg, and L. Hultman: *Thin Solid Films*, 2010, vol. 518, pp. 1851–78.
29. G.M. Song, V. Schnabel, C. Kwakernaak, S. Van der Zwaag, J.M. Schneider, and W.G. Sloof: *Mater. High Temp.*, 2012, vol. 29, pp. 205–09.
30. H.B. Zhang, Y.W. Bao, and Y.C. Zhou: *J. Mater. Sci. Technol.*, 2009, vol. 25, pp. 1–38.
31. J.P. Mazzoccoli, E.J. Lahoda and P. Xu: US Patent App. 13/670,808, 2012.
32. K.G. Field, X. Hu, K. Littrell, Y. Yamamoto, and L.L. Snead: *J. Nucl. Mater.*, 2015, vol. 465, pp. 746–55.
33. F.H. Stott, G.C. Wood, and J. Stringer: *Oxid. Met.*, 1995, vol. 44, pp. 113–45.
34. Y. Yamamoto, B.A. Pint, K.A. Terrani, K.G. Field, Y. Yang, and L.L. Snead: *J. Nucl. Mater.*, in press.
35. B.A. Pint, S. Dryepondt, K.A. Unocic, and D.T. Hoelzer: *JOM*, 2014, vol. 66, pp. 2458–66.
36. K.A. Unocic, D.T. Hoelzer, and B.A. Pint: *Mater. High Temp.*, 2015, vol. 32, pp. 123–32.
37. E.A. Gulbransen and K.F. Andrew: *J. Electrochemical Society*, 1959, vol. 106, pp. 294–302.
38. C.S. Wukusick and J.F. Collins: *Materials Research Standard*, 1964, vol. 4, pp. 637–46.
39. B.A. Pint, S. Dryepondt, A. Rouaix-Vande Put, and Y. Zhang: *JOM*, 2012, vol. 64, pp. 1454–60.